

# Machine learning meets $\mathfrak{su}(n)$ Lie algebra: Enhancing quantum dynamics learning with exact trace conservation

Arif Ullah<sup>1, a)</sup> and Jeremy O. Richardson<sup>2, b)</sup>

<sup>1)</sup>*School of Physics and Optoelectronic Engineering, Anhui University, Hefei, 230601, Anhui, China*

<sup>2)</sup>*Department of Chemistry and Applied Biosciences, ETH Zürich, 8093 Zürich, Switzerland*

(Dated: 24 February 2025)

Machine learning (ML) has emerged as a promising tool for simulating quantum dissipative dynamics. However, existing methods often struggle to enforce key physical constraints, such as trace conservation, when modeling reduced density matrices (RDMs). While Physics-Informed Neural Networks (PINN) aim to address these challenges, they frequently fail to achieve full physical consistency. In this work, we introduce a novel approach that leverages the  $\mathfrak{su}(n)$  Lie algebra to represent RDMs as a combination of an identity matrix and  $n^2 - 1$  Hermitian, traceless, and orthogonal basis operators, where  $n$  is the system's dimension. By learning only the coefficients associated with this basis, our framework inherently ensures exact trace conservation, as the traceless nature of the basis restricts the trace contribution solely to the identity matrix. This eliminates the need for explicit trace-preserving penalty terms in the loss function, simplifying optimization and improving learning efficiency. We validate our approach on two benchmark quantum systems: the spin-boson model and the Fenna-Matthews-Olson complex. By comparing the performance of four neural network (NN) architectures—Purely Data-driven Physics-Uninformed Neural Networks (PUNN),  $\mathfrak{su}(n)$  Lie algebra-based PUNN ( $\mathfrak{su}(n)$ -PUNN), traditional PINN, and  $\mathfrak{su}(n)$  Lie algebra-based PINN ( $\mathfrak{su}(n)$ -PINN)—we highlight the limitations of conventional methods and demonstrate the superior accuracy, robustness, and efficiency of our approach in learning quantum dissipative dynamics.

## I. INTRODUCTION

Open quantum systems provide a powerful framework for understanding the dynamics of quantum systems interacting with their environment. Such interactions are fundamental across various fields, including quantum information processing,<sup>1</sup> quantum memory,<sup>2</sup> quantum transport,<sup>3</sup> energy transfer in photosynthesis,<sup>4</sup> and biochemical processes like proton tunneling in DNA.<sup>5</sup> To describe these interactions, the total quantum state is typically divided into two components: the system of interest and its surrounding environment. The system's behavior is captured by the reduced density matrix (RDM), which evolves due to both the system's intrinsic dynamics and the influence of the environment.

Modeling environmental effects within the system dynamics presents significant challenges due to the vast number of environmental degrees of freedom. Approaches to model these effects range from mixed quantum-classical treatments<sup>6–17</sup> to entirely quantum descriptions.<sup>18</sup> In the mixed quantum-classical methods, the system is treated quantum mechanically, whereas the degrees of freedom of the environment, such as molecular vibrations, solvent motions, or other large-scale interactions, are represented by a classical phase space. Trajectories evolve according to classical equations of motion, typically derived from Newtonian or

Hamiltonian mechanics. This significantly reduces the computational complexity because it bypasses the high-dimensional Hilbert space of the environment.

Fully quantum approaches, in contrast, treat both the system and its environment within the quantum Hilbert space, allowing for a complete description of quantum coherence, dissipation, and entanglement in the system's dynamics. These methods capture the full quantum nature of the interactions without relying on classical approximations. Path-integral approaches like the hierarchical equations of motion (HEOM)<sup>19–26</sup> and quasiadiabatic propagator path integral (QUAPI)<sup>20,27</sup> rigorously incorporate memory effects and non-Markovian behavior. Quantum master equation methods, including the stochastic equation of motion (SEOM)<sup>28–33</sup> and the generalized master equation<sup>34,35</sup> provide alternative fully quantum descriptions of environmental interactions.

Although both mixed quantum-classical and fully quantum methods provide a thorough description of open quantum systems, they come with their own set of challenges. Classical approaches, for example, may fail to capture detailed balance<sup>36–38</sup> or subtle quantum correlations.<sup>39</sup> In contrast, while fully quantum methods offer a more accurate and complete representation of system-environment interactions, they often demand substantial computational resources, especially in scenarios involving strong system-environment coupling or when fine discretization steps are required to maintain numerical stability.

In recent years, machine learning (ML) has emerged as a powerful tool for learning complex spatio-temporal dynamics in high-dimensional spaces.<sup>40–61</sup> It has demon-

<sup>a)</sup>Electronic mail: arif@ahu.edu.cn

<sup>b)</sup>Electronic mail: jeremy.richardson@phys.chem.ethz.ch

strated proficiency in predicting the future evolution of quantum states based on historical data, as well as directly forecasting quantum states as a function of time and/or simulation parameters.

Despite the advantages of ML approaches, most methods directly learn and predict the dynamics of the individual RDM matrix elements, which often results in the violation of the fundamental physical principle of trace conservation. While physics-informed neural networks (PINN), which incorporate trace conservation into their loss function, help to mitigate trace violations, they still fail to fully preserve trace conservation, as demonstrated in our recent work.<sup>62</sup>

Taking inspiration from the success of the spin-mapping approach,<sup>10</sup> in this paper, we utilize the  $\mathfrak{su}(n)$  Lie algebra to expand the RDM  $\rho_S$  in terms of the identity operator and  $n^2 - 1$  traceless operators. The key point is that for a properly normalized RDM, the coefficient of the identity operator remains constant under exact quantum-mechanical evolution. We therefore only have to learn the  $n^2 - 1$  time-dependent coefficients corresponding to the traceless operators.

This approach offers significant advantages over directly learning the dynamics of the RDM. By focusing on the coefficients associated with the traceless operators, we inherently eliminate the need to account for trace conservation in the loss function, as these operators are traceless and the identity operator explicitly ensures the correct trace. This guarantees that the reconstructed RDM will always have the correct trace, unlike approaches such as PINN, which often struggle to enforce trace conservation during training. This inherent trace preservation simplifies the loss function, reducing its complexity and thereby enhancing the learning process and model performance.

## II. THEORY AND METHODOLOGY

Consider an open quantum system, denoted by  $S$ , with  $n$  states interacting with an external environment  $E$ . The dynamics of the combined system  $S + E$  is described by the Liouville–von-Neumann equation (assuming  $\hbar = 1$ ):

$$\dot{\rho}(t) = -i[\mathbf{H}, \rho(t)], \quad (1)$$

where  $\mathbf{H}$  is the Hamiltonian and  $\rho(t)$  is the density matrix of the total system. Given that this system is closed, it follows a unitary evolution. Assuming an initial state that is separable between the system and environment ( $\rho(0) = \rho_S(0) \otimes \rho_E(0)$ ), we can derive the system’s non-unitary reduced dynamics by taking a partial trace over the environmental degrees of freedom:

$$\begin{aligned} \rho_S(t) &= \mathbf{Tr}_E (\mathbf{U}(t, 0)\rho(0)\mathbf{U}^\dagger(t, 0)) \\ &= -i[\mathbf{H}_S, \rho_S(t)] + \mathcal{R}[\rho_S(t)], \end{aligned} \quad (2)$$

where  $\rho_S(t)$  is the RDM of the system at time  $t$ ,  $\mathbf{Tr}_E$  denotes the partial trace over the environment,  $\mathcal{R}$  is a super-operator that encodes the effects of the environment and

$\mathbf{U}(t, 0)$  and  $\mathbf{U}^\dagger(t, 0)$  are the forward and backward time-evolution operators, respectively. Though most physical systems interact with some environment, exact solutions often become infeasible due to the exponential growth in complexity—a phenomenon known as the “curse of dimensionality”. Below, we introduce two commonly studied open quantum systems: the two-state spin-boson (SB) model and the Fenna-Matthews-Olson (FMO) complex.

*SB model:* The SB model describes a qubit, or two-state system, coupled to a surrounding bath of independent harmonic oscillators. The Hamiltonian of the system, expressed in the basis of the excited ( $|e\rangle$ ) and ground ( $|g\rangle$ ) states, is:

$$H = \epsilon\sigma_z + \Delta\sigma_x + \sum_k \omega_k \mathbf{b}_k^\dagger \mathbf{b}_k + \sigma_z \sum_k c_k (\mathbf{b}_k^\dagger + \mathbf{b}_k), \quad (3)$$

where  $\sigma_z$  and  $\sigma_x$  are Pauli matrices,  $\epsilon$  is the energy difference between the two states, and  $\Delta$  denotes their coupling strength. The environment consists of harmonic modes with creation and annihilation operators  $\mathbf{b}_k^\dagger$  and  $\mathbf{b}_k$  for each mode  $k$ , which has a frequency  $\omega_k$ . The interaction between the system and the environment is characterized by a coupling constant  $c_k$  for each mode. The environmental influence is quantified by Debye spectral density:

$$J(\omega) = 2\lambda \frac{\gamma\omega}{\omega^2 + \gamma^2}, \quad (4)$$

where  $\lambda$  is the reorganization energy and  $\gamma$  is the characteristic frequency or the inverse of the relaxation time ( $\gamma = 1/\tau$ ).

*FMO Complex:* The FMO complex is a trimeric protein in green sulfur bacteria, critical to energy transfer in photosynthesis. Each monomer in the FMO complex includes several chlorophyll sites, typically seven or eight, which mediate energy transport. The dynamics within each monomer can be described by the Frenkel exciton model Hamiltonian:

$$\begin{aligned} \mathbf{H} &= \sum_{i=1}^n |i\rangle \epsilon_i \langle i| + \sum_{i \neq j}^n |i\rangle J_{ij} \langle j| \\ &+ \sum_{i=1}^j \sum_{k=1}^j \left( \frac{1}{2} \mathbf{P}_{k,i}^2 + \frac{1}{2} \omega_{k,i}^2 \mathbf{Q}_{k,i}^2 \right) \mathbf{I} \\ &- \sum_{i=1}^n \sum_{k=1}^n |i\rangle c_{k,i} \mathbf{Q}_{k,i} \langle i| + \sum_{i=1}^n |i\rangle \lambda_i \langle i|, \end{aligned} \quad (5)$$

where  $n$  is the number of chlorophyll sites,  $\epsilon_i$  is the site energy, and  $J_{ij}$  is the coupling between sites  $i$  and  $j$ . Here,  $\mathbf{P}_{k,i}$  and  $\mathbf{Q}_{k,i}$  are the momentum and position of the  $k$ -th mode interacting with site  $i$ , with  $\omega_{k,i}$  representing the frequency of each mode. The  $n \times n$  identity matrix  $\mathbf{I}$  ensures dimensional consistency in the model.  $c_{k,i}$

is the coupling constant between the  $k$ -th environmental mode and site  $i$ , and  $\lambda_i$  is the reorganization energy for site  $i$ .

For FMO complex, we use the Debye spectral density (Eq. (4)), assuming it is identical for all sites.

### A. ML-enhanced quantum dissipative dynamics

In the machine learning framework, modeling the time evolution of an open quantum system with an  $n$ -dimensional Hilbert space can be viewed as learning a mapping function. This function, denoted as  $\mathcal{M}$ , takes a set of input descriptors and maps them to either a single RDM or a sequence of RDMs. Mathematically, this can be expressed as:

$$\mathcal{M} : \{\mathbb{R}^{i \times j}\}^k \rightarrow \{\mathbb{R}^{n \times n}\}^l, \quad (6)$$

where  $\{\mathbb{R}^{i \times j}\}^k$  represents a collection of  $k$  input matrices, each of size  $i \times j$ , which encode relevant physical information such as past history, initial conditions and simulation parameters. The output,  $\{\mathbb{R}^{n \times n}\}^l$ , consists of  $l$  predicted RDMs, each of size  $n \times n$ , corresponding to different time steps. ML-based approaches developed so far can be divided into two main categories: recursive and non-recursive approaches, distinguished by the input descriptors and dynamics prediction.

*Recursive approaches:* Recursive ML strategies<sup>40,43,44,60</sup> predict future dynamics based on their historical data, resembling traditional quantum dynamics where the evolution at any time step depends explicitly on the current state and implicitly on prior states. The recursive mapping function, denoted as  $\mathcal{M}_{\text{rec}}$ , is defined as:

$$\mathcal{M}_{\text{rec}} : \{\mathbb{R}^{n \times n}\}^k \rightarrow \mathbb{R}^{n \times n} \quad (7)$$

such that

$$\mathcal{M}_{\text{rec}} [\rho_S(t_{k-k'}), \rho_S(t_{k-k'+1}), \dots, \rho_S(t_k)] = \rho_S(t_{k+1}), \quad (8)$$

where  $\mathcal{M}_{\text{rec}}$  takes a sequence of  $k'$  previous RDMs,  $\{\rho_S(t_j)\}_{j=k-k'}^k$ , representing a short trajectory of the system's past evolution. The function then predicts the RDM at the next time step,  $\rho_S(t_{k+1}) \in \mathbb{R}^{n \times n}$ . This process is applied iteratively: at each step, the newly predicted RDM is appended to the sequence, while the oldest entry is discarded, maintaining a fixed memory size of  $k'$  past time steps.

*Non-recursive approaches:* Non-recursive approaches<sup>41,42</sup> establish the mapping function  $\mathcal{M}$  as a direct relationship between simulation parameters (e.g., time, temperature, coupling strength, initial conditions) and system dynamics, bypassing reliance on prior states. Non-recursive approaches can be further divided into two categories: time-dependent non-recursive approaches and time-independent non-recursive approaches. The former approaches employ a

mapping function,  $\mathcal{M}_{\text{AIQD}}$ , that depends explicitly on time  $t$  and simulation parameters, defined as:

$$\mathcal{M}_{\text{AIQD}} : \mathbb{R} \times \mathbb{R}^p \rightarrow \mathbb{R}^{n \times n}, \quad (9)$$

such that

$$\mathcal{M}_{\text{AIQD}}(t, \mathbf{p}) = \rho_S(t), \quad (10)$$

where  $\mathbf{p}$  is a vector of simulation parameters. This methodology facilitates parallel computation of RDMs across all time steps, as each prediction is independent of prior results. The later time-independent non-recursive approaches,<sup>42</sup> on the other hand, determine the full RDM trajectory over a sequence of time steps in a single inference step. This is expressed as:

$$\mathcal{M}_{\text{OSTL}} : \mathbb{R}^p \rightarrow \{\mathbb{R}^{n \times n}\}^k, \quad (11)$$

such that

$$\mathcal{M}_{\text{OSTL}}(\mathbf{p}) = [\rho_S(t_1), \rho_S(t_2), \dots, \rho_S(t_k)], \quad (12)$$

where  $\mathbf{p}$  contains only the simulation parameters, and the model predicts the RDM trajectory for all specified time steps,  $t_1, t_2, \dots, t_k$ , in one computation. This approach streamlines trajectory prediction by eliminating the dependence on sequential steps.

### B. Expansion of RDM in traceless basis

The RDM  $\rho_S$  for a two-level quantum system can be elegantly expressed within the framework of  $\mathfrak{su}(2)$ , the Lie group of special unitary transformations in two dimensions. In this context,  $\rho_S$  is decomposed as a linear combination of the identity operator and the generators of the  $\mathfrak{su}(2)$  Lie algebra, the Pauli matrices:

$$\rho_S = a_0 \mathbf{I} + a_x \sigma_x + a_y \sigma_y + a_z \sigma_z = a_0 \mathbf{I} + \mathbf{a} \cdot \boldsymbol{\sigma}, \quad (13)$$

where  $a_0, a_x, a_y$ , and  $a_z$  are real coefficients, and  $\mathbf{a} = (a_x, a_y, a_z)$  serves as a time-dependent vector of coefficients. The basis elements (generators)  $\boldsymbol{\sigma} = (\sigma_x, \sigma_y, \sigma_z)$  are traceless Hermitian matrices:

$$\sigma_x = \frac{1}{2} \begin{pmatrix} 0 & 1 \\ 1 & 0 \end{pmatrix}, \quad \sigma_y = \frac{1}{2} \begin{pmatrix} 0 & -i \\ i & 0 \end{pmatrix}, \quad \sigma_z = \frac{1}{2} \begin{pmatrix} 1 & 0 \\ 0 & -1 \end{pmatrix}. \quad (14)$$

The decomposition above reflects the structure of  $\mathfrak{su}(2)$ , with  $\mathbf{I}$  as the trivial (identity) representation. Three key mathematical properties of the  $\mathfrak{su}(2)$  algebra are fundamental to this formulation: (1) The generators of  $\mathfrak{su}(2)$ ,  $\sigma_i$ , are traceless, i.e.,  $\text{Tr}[\sigma_i] = 0$ . In contrast, the identity matrix  $\mathbf{I}$  has  $\text{Tr}[\mathbf{I}] = 2$ . This tracelessness ensures that the coefficient  $a_0 = 1/n$  determines the trace of  $\rho_S$ , while the remaining coefficients,  $a_x, a_y, a_z$  correspond to the traceless part of  $\rho_S$ . This separation into

trace and traceless components arises naturally from the  $\mathfrak{su}(2)$  structure; (2) The Pauli matrices are orthogonal under the trace inner product, i.e.,  $\mathbf{Tr}[\sigma_i \sigma_j] = \frac{1}{2} \delta_{ij}$ . This orthogonality implies that the coefficients  $a_x, a_y, a_z$  are uniquely determined by projecting  $\rho_S$  onto the basis elements of  $\mathfrak{su}(2)$ , i.e.,  $a_i = 2\mathbf{Tr}[\rho_S \sigma_i]$ ; (3) The quadratic Casimir operator, which is central to the representation theory of  $\mathfrak{su}(2)$ , takes the form:

$$\sum_{i=1}^3 \sigma_i^2 = \frac{3}{4} \mathbf{I}. \quad (15)$$

This result reflects the fact that the sum of the squares of the generators is proportional to the identity operator.

Building upon the formalism developed for two-level systems ( $n = 2$ ), we now generalize the representation of the RDM and associated operators to  $n$ -level quantum systems. This extension utilizes the mathematical framework of the  $\mathfrak{su}(n)$  Lie algebra. In such systems, any Hermitian  $n \times n$  matrix can be expressed as a linear combination of the identity matrix  $\mathbf{I}$  and the traceless generators of  $\mathfrak{su}(n)$ . This decomposition is given by:

$$\rho_S = a_0 \mathbf{I} + \sum_{i=1}^{n^2-1} a_i \mathfrak{S}_i, \quad (16)$$

where  $\mathbf{I}$  is the  $n \times n$  identity matrix,  $\mathfrak{S}_i$  ( $i = 1, \dots, n^2-1$ ) are traceless Hermitian matrices that serve as the generators of  $\mathfrak{su}(n)$ , and  $a_i$  are coefficients encoding the system dynamics. These generators satisfy the same orthogonality relations as those in the  $\mathfrak{su}(2)$  algebra,  $\mathbf{tr}[\mathfrak{S}_i \mathfrak{S}_j] = \frac{1}{2} \delta_{ij}$ .

Furthermore, the quadratic Casimir operator maintains the same proportionality relationship with the identity operator as in the  $\mathfrak{su}(2)$  case:

$$\sum_{i=1}^{n^2-1} \mathfrak{S}_i^2 = \frac{n^2-1}{2n} \mathbf{I}. \quad (17)$$

This operator is invariant under unitary transformations and independent of the specific choice of  $\mathfrak{su}(n)$  basis, highlighting the universal properties of the Lie algebra representation.

The  $\mathfrak{su}(n)$  basis (generators) can be constructed as a generalization of the Pauli matrices from  $\mathfrak{su}(2)$  and is systematically divided into three categories:  $n(n-1)/2$  symmetric off-diagonal matrices,  $n(n-1)/2$  antisymmetric off-diagonal matrices, and  $n-1$  diagonal matrices. The symmetric off-diagonal basis are defined as:

$$\mathfrak{S}_{ij}^+ = \frac{1}{2} (|i\rangle \langle j| + |j\rangle \langle i|), \quad 1 \leq i < j \leq n, \quad (18)$$

while the antisymmetric off-diagonal basis are given by:

$$\mathfrak{S}_{ij}^- = -\frac{i}{2} (|i\rangle \langle j| - |j\rangle \langle i|), \quad 1 \leq i < j \leq n. \quad (19)$$

The diagonal basis are constructed as:

$$\mathfrak{S}_j = \sqrt{\frac{1}{2j(j-1)}} \left( \sum_{k=1}^{j-1} |k\rangle \langle k| + (1-j) |j\rangle \langle j| \right), \quad 2 \leq j \leq n. \quad (20)$$

It is important to emphasize that this choice for the  $\mathfrak{su}(n)$  basis is not unique. Any traceless Hermitian basis that satisfies the commutation and normalization conditions can be employed.

### III. RESULTS AND DISCUSSION

To showcase the effectiveness of our approach, we examine the relaxation dynamics of the SB model and exciton energy transfer (EET) in the FMO complex. We train three machine learning models: Purely Data-driven Physics-Uninformed Neural Networks (PUNN),  $\mathfrak{su}(n)$ -based PUNN ( $\mathfrak{su}(n)$ -PUNN), Physics-Informed Neural Networks (PINN), and  $\mathfrak{su}(n)$ -based PINN ( $\mathfrak{su}(n)$ -PINN). All models employ a hybrid architecture comprising convolutional neural networks (CNN), followed by LSTM layers, and fully connected dense layers (CNN-LSTM). Optimization was carried out using a composite loss function given, in general, by

$$\mathcal{L} = \alpha_1 \mathcal{L}_1 + \alpha_2 \mathcal{L}_2 + \alpha_3 \mathcal{L}_3 + \alpha_4 \mathcal{L}_4 + \alpha_5 \mathcal{L}_5, \quad (21)$$

where each term is defined as follows. The term  $\mathcal{L}_1$  represents the mean squared error (MSE) between the predicted ( $\rho_S$ ) and reference ( $\tilde{\rho}_S$ ) RDM's elements,

$$\mathcal{L}_1 = \frac{1}{N_t \cdot n^2} \sum_{t=1}^{N_t} \sum_{i,j=1}^n (\tilde{\rho}_{S,ij}(t) - \rho_{S,ij}(t))^2, \quad (22)$$

where  $N_t$  is the number of time steps. The term  $\mathcal{L}_2$  enforces the trace constraint by penalizing deviations of the trace of the predicted RDMs from unity,

$$\mathcal{L}_2 = \frac{1}{N_t} \sum_{t=1}^{N_t} (\mathbf{Tr} \rho_S(t) - 1)^2. \quad (23)$$

To ensure that the predicted RDMs are Hermitian, the deviation from Hermitian symmetry is penalized as:

$$\mathcal{L}_3 = \frac{1}{N_t \cdot n^2} \sum_{t=1}^{N_t} \sum_{i,j=1}^n |\rho_{S,ij}(t) - \rho_{S,ji}(t)^*|^2. \quad (24)$$

The term  $\mathcal{L}_4$  ensures positive semi-definiteness of the density matrix by penalizing negative eigenvalues  $\mu_i(t)$ ,

$$\mathcal{L}_4 = \frac{1}{N_t \cdot n} \sum_{t=1}^{N_t} \sum_{i=1}^n \max(0, -\mu_i(t))^2, \quad (25)$$

and  $\mathcal{L}_5$  constrains the eigenvalues to remain within the range  $[0, 1]$ , a fundamental property of all realistic RDMs.

$$\mathcal{L}_5 = \frac{1}{N_t \cdot n} \sum_{t=1}^{N_t} \sum_{i=1}^n (\text{clip}(\mu_i(t), 0, 1) - \mu_i(t))^2, \quad (26)$$

where the clip function clips  $\mu_i(t)$  to the interval  $[0, 1]$

$$\text{clip}(\mu_i(t), 0, 1) = \begin{cases} 0, & \text{if } \mu_i(t) < 0, \\ \mu_i(t), & \text{if } 0 \leq \mu_i(t) \leq 1, \\ 1, & \text{if } \mu_i(t) > 1. \end{cases} \quad (27)$$

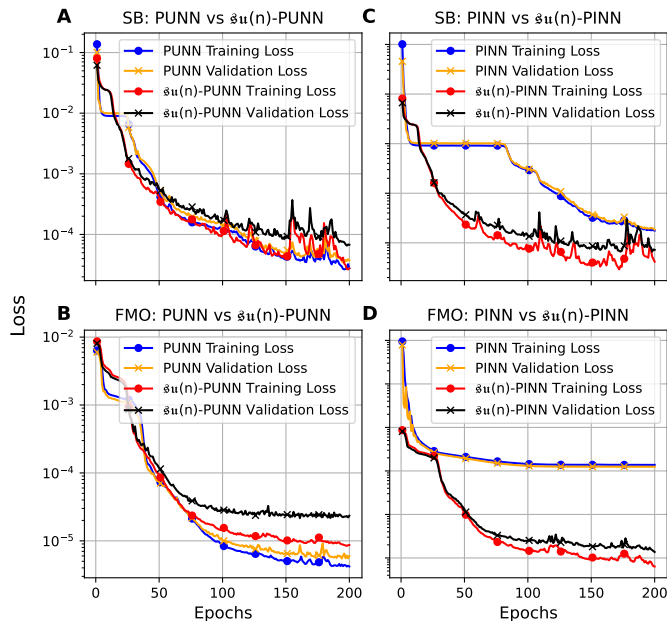


FIG. 1. Comparison of training and validation losses for PUNN,  $\mathfrak{su}(n)$ -PUNN, PINN, and  $\mathfrak{su}(n)$ -PINN as a function of the number of epochs.

The coefficients  $\alpha_1, \alpha_2, \alpha_3, \alpha_4, \alpha_5$  are tuning parameters that determine the relative contributions of the respective loss terms. Together, the terms  $\mathcal{L}_1, \mathcal{L}_2, \mathcal{L}_3, \mathcal{L}_4$  and  $\mathcal{L}_5$  ensure the validity of the RDM by enforcing accuracy, trace conservation, hermiticity, positive semi-definiteness, and eigenvalue constraints, respectively. For both the PUNN and  $\mathfrak{su}(n)$ -PUNN models, only  $\mathcal{L}_1$  is included with  $\alpha_1 = 1$  and  $\alpha_2 = \alpha_3 = \alpha_4 = \alpha_5 = 0$ , meaning no explicit physical constraints are applied. In the case of PINN, all constraints are employed with  $\alpha_1 = \alpha_2 = 1.0$ ,  $\alpha_3 = 2.0$  and  $\alpha_4 = \alpha_5 = 3.0$ . Similarly, the  $\mathfrak{su}(n)$ -PINN model incorporates  $\mathcal{L}_1, \mathcal{L}_3, \mathcal{L}_4$  and  $\mathcal{L}_5$  with the same tuned values as for PINN. Trace conservation is inherently satisfied in this case due to the properties of the  $\mathfrak{su}(n)$  Lie algebra representation, eliminating the need for  $\mathcal{L}_2$  (i.e.,  $\alpha_2 = 0$ ).

To train our models, for the SB model, the training data were sourced from the publicly accessible

QD3SET-1 database,<sup>63</sup> which provides precomputed RDMs via the hierarchical equations of motion (HEOM) approach.<sup>19,24,64,65</sup> The dataset, denoted as  $\mathcal{D}_{\text{sb}}$ , includes 1000 simulations over a four-dimensional parameter space ( $\varepsilon/\Delta, \lambda/\Delta, \gamma/\Delta$ , and  $\beta\Delta$ ) that defines the system-bath coupling strength, bath reorganization energy, bath relaxation rate, and inverse temperature. Similarly, for the seven-site FMO complex, data from the QD3SET-1 database were used. This dataset consists of 1000 simulations describing the dynamics for initial excitations at site-1 and site-6, spanning a parameter space ( $\lambda, \gamma, T$ ). Dynamics were propagated using the trace-conserving local thermalizing Lindblad master equation (LTLME),<sup>66</sup> with the Hamiltonian parameterized based on the work of Adolphs and Renger.<sup>67</sup>

To train the models, we employed OSTL-based dynamics propagation where RDM  $\rho_S(t)$  and coefficients  $a_i$  at each time step was converted into a 1D vector. In both PUNN and PINN models, the Hermitian property  $\rho_{S,ij}(t) = \rho_{S,ji}(t)^*$  is explicitly utilized. Consequently, only the diagonal elements (considering their real parts) and the upper off-diagonal elements were included in the analysis, with the real and imaginary components of the off-diagonal terms treated separately. In fact, because of this the loss-function term  $\mathcal{L}_3$  is zero by definition and can be neglected. Further methodological details can be found in Ref. 68. To optimize training process, farthest point sampling<sup>41,69</sup> was applied to select a subset of trajectories. For each case of the SB model ( $\varepsilon/\Delta = 0$  and 1) and the FMO complex (site-1 and 6), 400 trajectories were selected for training, and the remaining data were reserved for testing. Separate CNN-LSTM models were trained for the SB model and the FMO complex, each using an identical architecture. For comparison, we selected models with comparable training and validation losses.

To evaluate the learning efficiency of all models, Fig. 1 presents the learning curves, illustrating the decrease in loss versus training epochs for each model. For the SB model, both PUNN and  $\mathfrak{su}(n)$ -PUNN exhibit comparable learning performance. However,  $\mathfrak{su}(n)$ -PINN demonstrates significantly superior learning efficiency across all epochs, with the loss function decreasing rapidly. In the case of the more complex FMO system, PUNN achieves a marginally lower loss compared to  $\mathfrak{su}(n)$ -PUNN. Nonetheless, similar to the SB model,  $\mathfrak{su}(n)$ -PINN outperforms PINN in terms of learning efficiency. These findings highlight that expanding the RDM in the  $\mathfrak{su}(n)$  basis simplifies optimization and enhances learning efficiency and can describe more physically realistic behavior.

Fig. 2 highlights the performance of trace conservation across the four models. The purely data-driven PUNN model fails entirely to conserve the trace in both cases. While PINN shows substantial improvement in trace conservation, minor violations still occur. This limitation stems from the fact that the physical constraints in the PINN loss function are considered to be "soft" con-

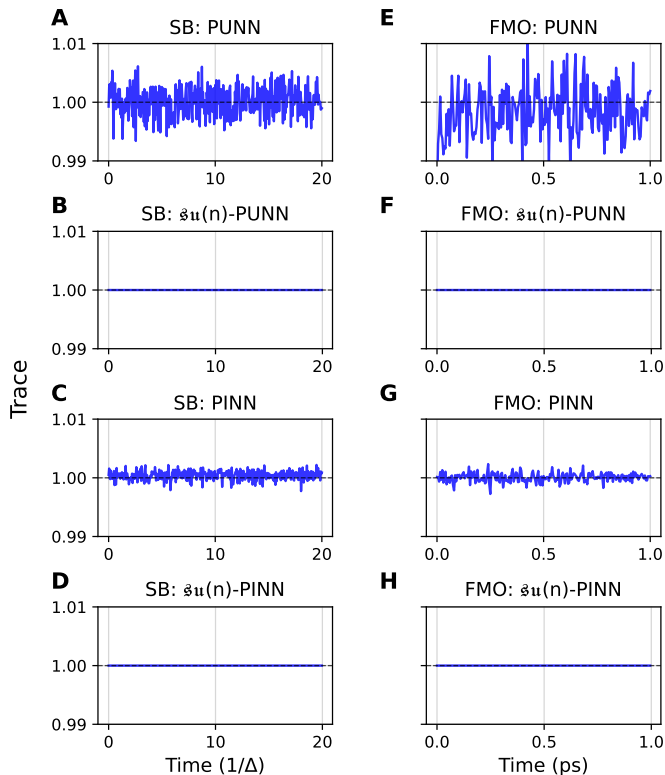


FIG. 2. Comparison of trace conservation in quantum dissipative dynamics using PUNN,  $\mathfrak{su}(n)$ -PUNN, PINN, and  $\mathfrak{su}(n)$ -PINN. The first column presents results for the asymmetric SB model, while the second column focuses on the FMO complex with initial excitation on site 1. For the SB model, the results correspond to an unseen dynamics characterized by  $\varepsilon/\Delta = 1.0$ ,  $\gamma/\Delta = 9.0$ ,  $\lambda/\Delta = 0.6$ , and  $\beta\Delta = 1.0$ . For the FMO complex, the parameters are  $\gamma = 400 \text{ cm}^{-1}$ ,  $\lambda = 40 \text{ cm}^{-1}$ , and  $T = 90 \text{ K}$ . Details on training and prediction are provided in the Results and Discussion section.

straints. As a result, they guide the training process but are not strictly enforced.<sup>62,70,71</sup> In contrast, the  $\mathfrak{su}(n)$ -PUNN and  $\mathfrak{su}(n)$ -PINN ensure the exact trace conservation by embedding the trace explicitly via the identity matrix, as a result achieving perfect trace preservation by design, rather than relying on the loss function.

Fig. 3 evaluates the positive semi-definiteness and eigenvalue constraints of the predicted RDMs by analyzing their eigenvalues. For simpler systems, such as the SB model, all models perform similarly, with nearly all eigenvalues remaining positive, except for a few negative eigenvalues in the PUNN results. In more complex cases, like the FMO complex, the PUNN model produces approximately 13% negative eigenvalues (183 out of 1407), while PINN yields 3.6% negative eigenvalues (52 out of 1407), demonstrating that incorporating the loss terms  $\mathcal{L}_4$  and  $\mathcal{L}_5$  improves the positivity of the predicted RDMs. In contrast, the purely data-driven  $\mathfrak{su}(n)$ -PUNN results in only 0.78% negative eigenvalues (11 out of 1407), outperforming PINN even with all constraints included. Fi-

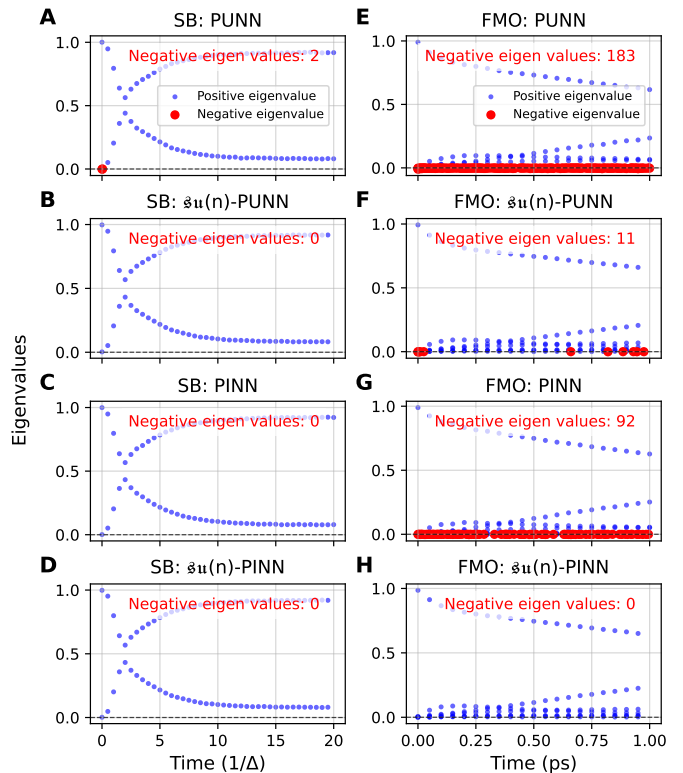


FIG. 3. Evaluation of positive semi-definiteness and eigenvalue constraints in the predicted RDMs across PUNN,  $\mathfrak{su}(n)$ -PUNN, PINN, and  $\mathfrak{su}(n)$ -PINN models. Sparse positive eigenvalues are shown for clarity, with simulation parameters consistent with those in Fig. 3. In the SB model (left column), all models produce predominantly positive eigenvalues, though minor deviations are present in PUNN. For the FMO complex (right column), the purely data-driven  $\mathfrak{su}(n)$ -PUNN results in only 0.78% negative eigenvalues (11 out of 1407), outperforming PINN even with all constraints included. By incorporating the corresponding loss terms in  $\mathfrak{su}(n)$ -PINN, all predicted RDMs achieve complete positivity.

nally, by adding the corresponding loss terms in  $\mathfrak{su}(n)$ -PINN, all predicted RDMs achieve complete positivity. This further confirms that our  $\mathfrak{su}(n)$  approach enhances learning efficiency.

TABLE I. Average mean absolute error (MAE) for the diagonal (Diag) and off-diagonal (Off-diag) elements of the RDM predicted by the PUNN,  $\mathfrak{su}(n)$ -PUNN, PINN, and  $\mathfrak{su}(n)$ -PINN models for the SB model and FMO complex. The off-diagonal errors include the average MAE for both the real and imaginary components.

Model	SB Model		FMO Complex	
	Diag	Off-diag (Real, Imag)	Diag	Off-diag (Real, Imag)
PUNN	0.0032	(0.0026, 0.0027)	0.0074	(0.0031, 0.0014)
$\mathfrak{su}(n)$ -PUNN	0.0020	(0.0011, 0.0013)	0.0056	(0.0019, 0.00077)
PINN	0.0027	(0.0028, 0.0018)	0.0092	(0.0021, 0.00072)
$\mathfrak{su}(n)$ -PINN	0.0017	(0.0014, 0.0014)	0.0037	(0.0014, 0.00071)

To further assess the performance of the four models,

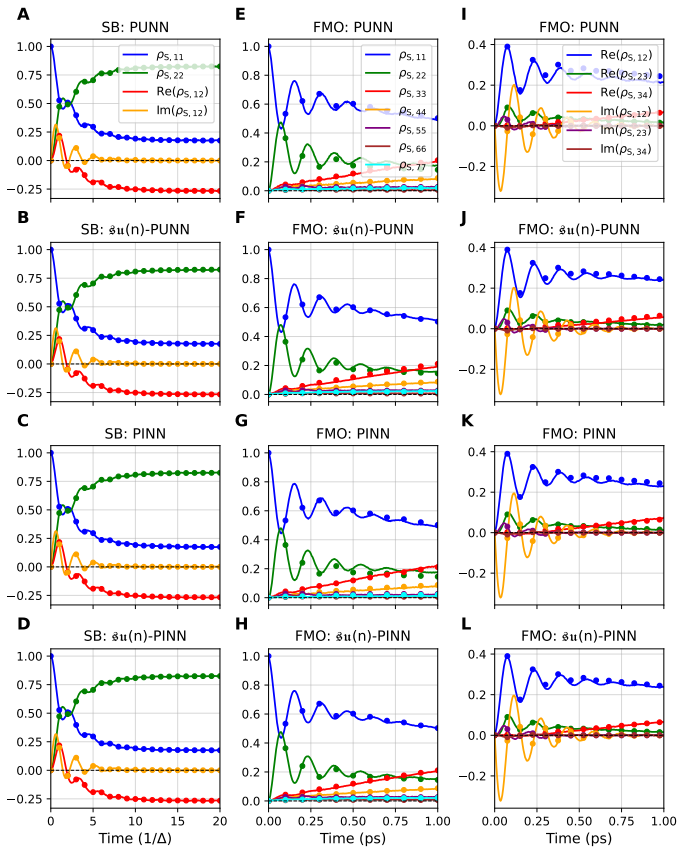


FIG. 4. Evolution of the RDM’s elements, including population and coherence terms, as predicted by PUNN,  $\mathfrak{su}(n)$ -PUNN, PINN, and  $\mathfrak{su}(n)$ -PINN models. The first column shows the relaxation dynamics for the SB model, while the second and third columns highlight the diagonal (population) and selected off-diagonal (coherence) elements of the RDM for the FMO complex, respectively. Simulation parameters are provided in the caption of Fig. 2 and accuracy comparison is given in Table I.

Table I compares the accuracy of PUNN,  $\mathfrak{su}(n)$ -PUNN, PINN, and  $\mathfrak{su}(n)$ -PINN in predicting the evolution of RDM elements (population and coherence terms) for the SB model and the FMO complex, as illustrated in Fig. 4. For the SB model, all models provide accurate predictions; however,  $\mathfrak{su}(n)$ -PUNN and  $\mathfrak{su}(n)$ -PINN achieve the lowest errors for both diagonal and off-diagonal elements, demonstrating superior learning capabilities compared to PUNN and PINN. Although PUNN and PINN also perform well, their errors are marginally higher.

In the case of the FMO complex,  $\mathfrak{su}(n)$ -PINN exhibits the best overall performance, followed by  $\mathfrak{su}(n)$ -PUNN. Similar to the SB model, PUNN and PINN show higher errors for both diagonal and off-diagonal terms.

#### IV. CONCLUDING REMARKS

In this work, we addressed the limitations of existing ML approaches for modeling RDM, particularly their challenges in learning efficiency and enforcing physical constraints such as trace conservation. Traditional methods often directly model the RDM, relying on nonlinear loss functions to maintain physical constraints, which can hinder optimization and lead to unphysical predictions.

To overcome these limitations, we introduced a novel approach that leverages the  $\mathfrak{su}(n)$  Lie algebra to expand the RDM in terms of an identity matrix and  $n^2 - 1$  operators, where  $n$  is the system’s dimension. These operators are Hermitian, traceless, orthogonal, and satisfy the quadratic Casimir operator condition. The traceless nature of the operators ensures that only the identity matrix contributes to the trace of the RDM, inherently guaranteeing exact trace conservation. Unlike methods such as PINN, which often struggle to enforce trace conservation during training, our approach eliminates the need for explicit penalty terms in the loss function, simplifying optimization and enhancing training stability. Additionally, we believe that the Lie-algebra approach provides a promising direction for generalizing training data to systems of varying dimensions.

In summary, our  $\mathfrak{su}(n)$  Lie algebra-based framework not only ensures exact trace conservation but also simplifies the learning process, reduces computational complexity, and enhances the scalability of ML models for quantum dynamics. This approach represents a significant step forward in the accurate and efficient modeling of quantum systems using machine learning.

#### V. ACKNOWLEDGMENTS

A.U. acknowledges funding from the National Natural Science Foundation of China (No. W2433037) and Natural Science Foundation of Anhui Province (No. 2408085QA002).

#### VI. DATA AVAILABILITY

The code and data supporting this work are available at [https://github.com/Arif-PhyChem/su\\_lie\\_algebra](https://github.com/Arif-PhyChem/su_lie_algebra).

#### VII. COMPETING INTERESTS

The authors declare no competing interests.

## REFERENCES

- <sup>1</sup>Breuer HP, Laine EM, Piilo J, Vacchini B. Colloquium: Non-Markovian dynamics in open quantum systems. *Reviews of Modern Physics*. 2016;88(2):021002.
- <sup>2</sup>Khodjasteh K, Sastrawan J, Hayes D, Green TJ, Biercuk MJ, Viola L. Designing a practical high-fidelity long-time quantum memory. *Nature Communications*. 2013;4(1):2045.
- <sup>3</sup>Cui P, Li XQ, Shao J, Yan Y. Quantum transport from the perspective of quantum open systems. *Physics Letters A*. 2006;357(6):449-53.
- <sup>4</sup>Zerah Harush E, Dubi Y. Do photosynthetic complexes use quantum coherence to increase their efficiency? Probably not. *Science advances*. 2021;7(8):eabc4631.
- <sup>5</sup>Slocombe L, Sacchi M, Al-Khalili J. An open quantum systems approach to proton tunnelling in DNA. *Communications Physics*. 2022;5(1):109.
- <sup>6</sup>Miller WH. The Semiclassical Initial Value Representation: A Potentially Practical Way for Adding Quantum Effects to Classical Molecular Dynamics Simulations. *J Phys Chem A*. 2001;105(13):2942-55.
- <sup>7</sup>Cotton SJ, Miller WH. Symmetrical windowing for quantum states in quasi-classical trajectory simulations: Application to electronically non-adiabatic processes. *The Journal of chemical physics*. 2013;139(23).
- <sup>8</sup>Liu J, He X, Wu B. Unified formulation of phase space mapping approaches for nonadiabatic quantum dynamics. *Accounts of chemical research*. 2021;54(23):4215-28.
- <sup>9</sup>Runeson JE, Richardson JO. Spin-mapping approach for nonadiabatic molecular dynamics. *The Journal of Chemical Physics*. 2019;151(4):044119.
- <sup>10</sup>Runeson JE, Richardson JO. Generalized spin mapping for quantum-classical dynamics. *The Journal of chemical physics*. 2020;152(8).
- <sup>11</sup>Mannouch JR, Richardson JO. A partially linearized spin-mapping approach for nonadiabatic dynamics. I. Derivation of the theory. *The Journal of chemical physics*. 2020;153(19).
- <sup>12</sup>Mannouch JR, Richardson JO. A partially linearized spin-mapping approach for nonadiabatic dynamics. II. Analysis and comparison with related approaches. *The Journal of chemical physics*. 2020;153(19).
- <sup>13</sup>Mannouch JR, Richardson JO. A partially linearized spin-mapping approach for simulating nonlinear optical spectra. *The Journal of Chemical Physics*. 2022;156(2).
- <sup>14</sup>Tao G. A multi-state trajectory method for non-adiabatic dynamics simulations. *The Journal of Chemical Physics*. 2016;144(9).
- <sup>15</sup>Mannouch JR, Richardson JO. A mapping approach to surface hopping. *The Journal of Chemical Physics*. 2023;158(10).
- <sup>16</sup>Crespo-Otero R, Barbatti M. Recent advances and perspectives on nonadiabatic mixed quantum-classical dynamics. *Chemical reviews*. 2018;118(15):7026-68.
- <sup>17</sup>Qiu J, Lu Y, Wang L. Multilayer subsystem surface hopping method for large-scale nonadiabatic dynamics simulation with hundreds of thousands of states. *Journal of Chemical Theory and Computation*. 2022;18(5):2803-15.
- <sup>18</sup>Ivander F, Lindoy LP, Lee J. Unified framework for open quantum dynamics with memory. *Nature Communications*. 2024;15(1):8087.
- <sup>19</sup>Tanimura Y, Kubo R. Time evolution of a quantum system in contact with a nearly Gaussian-Markoffian noise bath. *Journal of the Physical Society of Japan*. 1989;58(1):101-14.
- <sup>20</sup>Makarov DE, Makri N. Path integrals for dissipative systems by tensor multiplication. *Condensed phase quantum dynamics for arbitrarily long time*. *Chemical physics letters*. 1994;221(5-6):482-91.
- <sup>21</sup>Su Y, Chen ZH, Wang Y, Zheng X, Xu RX, Yan Y. Extended dissipaton equation of motion for electronic open quantum systems: Application to the Kondo impurity model. *The Journal of Chemical Physics*. 2023;159(2).
- <sup>22</sup>Yan Y, Xu M, Li T, Shi Q. Efficient propagation of the hierarchical equations of motion using the Tucker and hierarchical Tucker tensors. *The Journal of Chemical Physics*. 2021;154(19).
- <sup>23</sup>Gong H, Ullah A, Ye L, Zheng X, Yan Y. Quantum entanglement of parallel-coupled double quantum dots: A theoretical study using the hierarchical equations of motion approach. *Chinese Journal of Chemical Physics*. 2018;31(4):510.
- <sup>24</sup>Xu M, Yan Y, Shi Q, Ankerhold J, Stockburger J. Taming quantum noise for efficient low temperature simulations of open quantum systems. *Physical Review Letters*. 2022;129(23):230601.
- <sup>25</sup>Bai S, Zhang S, Huang C, Shi Q. Hierarchical Equations of Motion for Quantum Chemical Dynamics: Recent Methodology Developments and Applications. *Accounts of Chemical Research*. 2024;57(21):3151-60.
- <sup>26</sup>Wang Y, Mulvihill E, Hu Z, Lyu N, Shivpuje S, Liu Y, et al. Simulating open quantum system dynamics on NISQ computers with generalized quantum master equations. *Journal of Chemical Theory and Computation*. 2023;19(15):4851-62.
- <sup>27</sup>Makri N. Quantum Dynamics Methods Based on the Real-Time Path Integral. In: *Comprehensive Computational Chemistry, First Edition: Volume 1-4*. Elsevier; 2023. p. V4-293.
- <sup>28</sup>Han L, Chernyak V, Yan YA, Zheng X, Yan Y. Stochastic Representation of Non-Markovian Fermionic Quantum Dissipation. *Physical review letters*. 2019;123(5):050601.
- <sup>29</sup>Han L, Ullah A, Yan YA, Zheng X, Yan Y, Chernyak V. Stochastic equation of motion approach to fermionic dissipative dynamics. I. Formalism. *The Journal of Chemical Physics*. 2020;152(20):204105.
- <sup>30</sup>Ullah A, Han L, Yan YA, Zheng X, Yan Y, Chernyak V. Stochastic equation of motion approach to fermionic dissipative dynamics. II. Numerical implementation. *The Journal of Chemical Physics*. 2020;152(20):204106.
- <sup>31</sup>Chen L, Bennett DI, Eisfeld A. Simulation of absorption spectra of molecular aggregates: A hierarchy of stochastic pure state approach. *The Journal of Chemical Physics*. 2022;156(12).
- <sup>32</sup>Dan X, Xu M, Yan Y, Shi Q. Generalized master equation for charge transport in a molecular junction: Exact memory kernels and their high order expansion. *The Journal of Chemical Physics*. 2022;156(13).
- <sup>33</sup>Stockburger JT. Exact propagation of open quantum systems in a system-reservoir context. *EPL (Europhysics Letters)*. 2016;115(4):40010.
- <sup>34</sup>Lyu N, Mulvihill E, Soley MB, Geva E, Batista VS. Tensor-train thermo-field memory kernels for generalized quantum master equations. *Journal of Chemical Theory and Computation*. 2023;19(4):1111-29.
- <sup>35</sup>Liu Yy, Yan Ym, Xu M, Song K, Shi Q. Exact generator and its high order expansions in time-convolutionless generalized master equation: Applications to spin-boson model and excitation energy transfer. *Chinese Journal of Chemical Physics*. 2018;31(4):575-83.
- <sup>36</sup>Schmidt JR, Parandekar PV, Tully JC. Mixed quantum-classical equilibrium: Surface hopping. *J Chem Phys*. 2008;129(4):044104.
- <sup>37</sup>Amati G, Runeson JE, Richardson JO. On detailed balance in nonadiabatic dynamics: From spin spheres to equilibrium ellipsoids. *J Chem Phys*. 2023;158:064113.
- <sup>38</sup>Amati G, Mannouch JR, Richardson JO. Detailed balance in mixed quantum-classical mapping approaches. *J Chem Phys*. 2023;159:214114.
- <sup>39</sup>Mannouch JR, Kelly A. Toward a Correct Description of Initial Electronic Coherence in Nonadiabatic Dynamics Simulations. *J Phys Chem Lett*. 2024;15:11687-95.
- <sup>40</sup>Ullah A, Dral PO. Speeding up quantum dissipative dynamics of open systems with kernel methods. *New Journal of Physics*. 2021.
- <sup>41</sup>Ullah A, Dral PO. Predicting the future of excitation energy transfer in light-harvesting complex with artificial intelligence-based quantum dynamics. *Nature communications*.



- 2022;13(1930):1-8.
- <sup>42</sup>Ullah A, Dral PO. One-Shot Trajectory Learning of Open Quantum Systems Dynamics. *The Journal of Physical Chemistry Letters*. 2022;13(26):6037-41.
- <sup>43</sup>Rodríguez LEH, Ullah A, Espinosa KJR, Dral PO, Kananenka AA. A comparative study of different machine learning methods for dissipative quantum dynamics. *Machine Learning: Science and Technology*. 2022;3(4):045016.
- <sup>44</sup>Herrera Rodríguez LE, Kananenka AA. Convolutional neural networks for long time dissipative quantum dynamics. *The Journal of Physical Chemistry Letters*. 2021;12(9):2476-83.
- <sup>45</sup>Ge F, Zhang L, Hou YF, Chen Y, Ullah A, Dral PO. Four-dimensional-spacetime atomistic artificial intelligence models. *The Journal of Physical Chemistry Letters*. 2023;14(34):7732-43.
- <sup>46</sup>Zhang L, Ullah A, Pinheiro Jr M, Dral PO, Barbatti M. Excited-state dynamics with machine learning. In: *Quantum Chemistry in the Age of Machine Learning*. Elsevier; 2023. p. 329-53.
- <sup>47</sup>Wu D, Hu Z, Li J, Sun X. Forecasting nonadiabatic dynamics using hybrid convolutional neural network/long short-term memory network. *The Journal of Chemical Physics*. 2021;155(22):224104.
- <sup>48</sup>Lin K, Peng J, Xu C, Gu FL, Lan Z. Automatic evolution of machine-learning-based quantum dynamics with uncertainty analysis. *Journal of Chemical Theory and Computation*. 2022;18(10):5837-55.
- <sup>49</sup>Bandyopadhyay S, Huang Z, Sun K, Zhao Y. Applications of neural networks to the simulation of dynamics of open quantum systems. *Chemical Physics*. 2018;515:272-8.
- <sup>50</sup>Yang B, He B, Wan J, Kubal S, Zhao Y. Applications of neural networks to dynamics simulation of Landau-Zener transitions. *Chemical Physics*. 2020;528:110509.
- <sup>51</sup>Lin K, Peng J, Xu C, Gu FL, Lan Z. Trajectory Propagation of Symmetrical Quasi-classical Dynamics with Meyer-Miller Mapping Hamiltonian Using Machine Learning. *The Journal of Physical Chemistry Letters*. 2022;13:11678-88.
- <sup>52</sup>Tang D, Jia L, Shen L, Fang WH. Fewest-Switches Surface Hopping with Long Short-Term Memory Networks. *The Journal of Physical Chemistry Letters*. 2022;13(44):10377-87.
- <sup>53</sup>Shakiba M, Philips AB, Autschbach J, Akimov AV. Machine Learning Mapping Approach for Computing Spin Relaxation Dynamics. *The Journal of Physical Chemistry Letters*. 2024. In press.
- <sup>54</sup>Lin K, Gao X. Enhancing Open Quantum Dynamics Simulations Using Neural Network-Based Non-Markovian Stochastic Schrödinger Equation Method. *arXiv preprint arXiv:241115914*. 2024.
- <sup>55</sup>Zeng H, Kou Y, Sun X. How Sophisticated Are Neural Networks Needed to Predict Long-Term Nonadiabatic Dynamics? *Journal of Chemical Theory and Computation*. 2024;20(22):9832-48.
- <sup>56</sup>Long C, Cao L, Ge L, Li QX, Yan Y, Xu RX, et al. Quantum neural network approach to Markovian dissipative dynamics of many-body open quantum systems. *The Journal of Chemical Physics*. 2024 08;161(8):084105. Available from: <https://doi.org/10.1063/5.0220357>.
- <sup>57</sup>Cao L, Ge L, Zhang D, Li X, Wang Y, Xu RX, et al. Neural Network Approach for Non-Markovian Dissipative Dynamics of Many-Body Open Quantum Systems. *arXiv preprint arXiv:240411093*. 2024.
- <sup>58</sup>Zhang J, Chen L. A non-Markovian neural quantum propagator and its application in the simulation of ultrafast nonlinear spectra. *Phys Chem Chem Phys*. 2025;27:182-9. Available from: <http://dx.doi.org/10.1039/D4CP03736G>.
- <sup>59</sup>Zhang J, Benavides-Riveros CL, Chen L. Artificial-Intelligence-Based Surrogate Solution of Dissipative Quantum Dynamics: Physics-Informed Reconstruction of the Universal Propagator. *The Journal of Physical Chemistry Letters*. 2024;15(13):3603-10.
- <sup>60</sup>Herrera Rodríguez LE, Kananenka AA. A short trajectory is all you need: A transformer-based model for long-time dissipative quantum dynamics. *The Journal of Chemical Physics*. 2024;161(17).
- <sup>61</sup>Zhang J, Benavides-Riveros CL, Chen L. Neural quantum propagators for driven-dissipative quantum dynamics. *Phys Rev Res*. 2025 Jan;7:L012013. Available from: <https://link.aps.org/doi/10.1103/PhysRevResearch.7.L012013>.
- <sup>62</sup>Ullah A, Huang Y, Yang M, Dral PO. Physics-informed neural networks and beyond: enforcing physical constraints in quantum dissipative dynamics. *Digital Discovery*. 2024;3:2052-60.
- <sup>63</sup>Ullah A, Rodríguez LEH, Dral PO, Kananenka AA. QD3SET-1: A Database with Quantum Dissipative Dynamics Data Sets. *Frontiers in Physics*. 2023;11:1223973.
- <sup>64</sup>Shi Q, Chen L, Nan G, Xu RX, Yan Y. Efficient hierarchical Liouville space propagator to quantum dissipative dynamics. *The Journal of chemical physics*. 2009;130(8):084105.
- <sup>65</sup>Chen ZH, Wang Y, Zheng X, Xu RX, Yan Y. Universal time-domain Prony fitting decomposition for optimized hierarchical quantum master equations. *The Journal of Chemical Physics*. 2022;156:221102.
- <sup>66</sup>Mohseni M, Rebentrost P, Lloyd S, Aspuru-Guzik A. Environment-assisted quantum walks in photosynthetic energy transfer. *J Chem Phys*. 2008;129(17):11B603.
- <sup>67</sup>Adolphs J, Renger T. How proteins trigger excitation energy transfer in the FMO complex of green sulfur bacteria. *Biophysical journal*. 2006;91(8):2778-97.
- <sup>68</sup>Ullah A, Dral PO. MLQD: A package for machine learning-based quantum dissipative dynamics. *Computer Physics Communications*. 2024;294:108940.
- <sup>69</sup>Dral PO. MLatom: A program package for quantum chemical research assisted by machine learning. *Journal of computational chemistry*. 2019;40(26):2339-47.
- <sup>70</sup>Wang R, Yu R. Physics-guided deep learning for dynamical systems: A survey. *arXiv preprint arXiv:210701272*. 2021.
- <sup>71</sup>Norambuena A, Mattheakis M, González FJ, Coto R. Physics-informed neural networks for quantum control. *Physical Review Letters*. 2024;132(1):010801.